Carbon Letters (2021) 31:13–28
https://doi.org/10.1007/s42823-020-00145-x

Online ISSN 2233-4998
Print ISSN 1976-4251

ORIGINAL ARTICLE

High removal of emerging contaminants from wastewater by activated carbons derived from the shell of cashew of Para

Pascal S. Thue[1] · Diana R. Lima[2] · Mu Naushad[3] · Eder C. Lima[1,2,4] · Ytallo R. T. de Albuquerque[2] · Silvio L. P. Dias[1,4] · Mariene R. Cunha[2] · Guilherme L. Dotto[5] · Irineu A. S. de Brum[2,6]

Received: 6 January 2020 / Revised: 27 February 2020 / Accepted: 10 April 2020 / Published online: 15 May 2020

Abstract

Activated carbon from the shell of the cashew of Para (SCP) was produced by chemical activation with ZnCl using the ratio of SCP: $ZnCl_2$ 1.0:1.5 at 700 °C. The prepared activated carbon (SCP700) was used for the removal of two emerging contaminants, 4-bromophenol (4-BrPhOH) and 4-chloroaniline (4-$ClPhNH_2$) that are primarily employed in the industry. Different analytical techniques were used to characterize the activated carbon. From the N_2 adsorption–desorption isotherms were obtained the specific surface area of 1520 $m^2\ g^{-1}$ and total pore volume of 0.492 $cm^3\ g^{-1}$. The functional groups were identified by the FTIR technique and quantified by modified Boehm titration. The results revealed the bearing of several functional groups on the SCP700 surface, which may utterly influence the removal of the emerging contaminants. The equilibrium experiments showed that the maximum uptaken capacities (Q_{max}) achieved at 45 °C were 488.2 (4-BrPhOH) and 552.5 mg g^{-1} (4-$ClPhNH_2$). The thermodynamic parameters demonstrated that the processes of 4-BrPhOH and 4-ClPhNH2 adsorption are exothermic, spontaneous, energetically suitable, and the magnitude of ΔH° is compatible with physisorption. The mechanism of the adsorption of the emerging contaminants onto the carbon surface is dominated by microporous filling, hydrogen bonds, π-stacking interactions, and other Van der Waals interactions. The use of activated carbon for the treatment of industrial synthetic wastewater with several inorganic and organic molecules commonly found in industrial effluents showed a very high percentage of uptaking (up to 98.64%).

Keywords Emerging contaminants · Carbon adsorbent · Adsorption · Industrial wastewaters · Adsorption thermodynamics

1 Introduction

With the growth of population around the world, there is an increasing necessity for manufactured products, foodstuffs, clothes, and others. The production of these industrialized products generates several organic and inorganic pollutants

Electronic supplementary material The online version of this article (https://doi.org/10.1007/s42823-020-00145-x) contains supplementary material, which is available to authorized users.

✉ Pascal S. Thue
pascal.thue@ufrgs.br

✉ Eder C. Lima
profederlima@gmail.com

1 Graduate Science of Materials Program (PGCIMAT), Institute of Chemistry, Federal University of Rio Grande Do Sul (UFRGS), Av. Bento Gonçalves 9500, Porto Alegre, RS, Brazil

2 Graduate Mine, Metallurgical and Materials Engineering Program (PPGE3M), School of Engineering, Federal University of Rio Grande Do Sul (UFRGS), Av. Bento Gonçalves 9500, Porto Alegre, RS, Brazil

3 Department of Chemistry, College of Science, King Saud University, Riyadh 11451, Saudi Arabia

4 Institute of Chemistry, Federal University of Rio Grande Do Sul (UFRGS), Av. Bento Gonçalves 9500, P.O. Box 15003, Porto Alegre, RS 91501-970, Brazil

5 Chemical Engineering Department, Federal University of Santa Maria, UFSM, Santa Maria, RS, Brazil

6 Department of Metallurgical Engineering, Federal University of Rio Grande Do Sul (UFRGS), 9500 Bento Gonçalves Avenue, Porto Alegre 91501-970, Brazil

in different concentration ranges that could be released into the environment without any treatment or whose treatment is not suitable for complete removal before its disposal to waters [1].

Recently, new hazardous pollutants, called emerging contaminants (ECs), have featured in the scientific community [2–5]. ECs can be understood as any microorganism and any synthetic chemical or naturally occurring that is not conventionally quantified in the environment with possible ecological or health effects to humans [2–5]. The ECs consist of pharmaceuticals, personal care products, hormones, fuel additives, oil additives, flame retardants, pesticides, surfactants, plasticizers, solvents, and different industrial chemicals [1–5].

Most ECs come from industrial and municipal wastewater treatment plants, which are unable to remove these chemicals by the traditional treatment that cannot remove low concentrations of these chemicals [6, 7].

Different methods for treatment of wastewaters and waters containing ECs, for instance, biological treatments [8, 9], advanced oxidative process (AOP) [10–13], separation by membranes [7, 13–15], and adsorption [16–21] were reported elsewhere. Notwithstanding, many of the above-mentioned treatment methods have some shortcomings, such as the generation of sludge as byproducts and the high initial costs for implementation [1, 5]. On the other hand, adsorption used as a unit operation in the treatment of wastewater containing ECs shows some merits, such as the simple operation and low initial cost for execution [2, 20].

Among the most used materials employed for adsorption of ECs from aqueous media, the activated carbon (AC) appear as the best one due to some important characteristic such as high specific surface area and a high volume of pores. Those properties confer to AC outstanding adsorption capacities [20, 21]. AC adsorbents are produced from a different kind of carbon precursors [19–25], that generate carbon adsorbents with different quality and textural characteristics.

Using biomass residues in the preparation of porous materials such as activated carbons has risen considerably in the past years. Among the most used residual biomasses for the preparation of porous ACs are fruit wastes [20–22], pod wastes [19], pasturage [23], peat [24], and organic sludges [24, 25], and others.

Although the use of different plant biomasses has been used for the preparation of different activated carbons, the field of preparation of new carbon materials for the removal of emerging contaminants is still a fruitful area. In this research, the use of residual biomass of the shell of the cashew of Para (SCP) is proposed as a precursor for the fabrication of AC to valorize this waste-biomass, which is generated in high amounts and have no practical use in Brazil [26, 27]. The cashew of the Para residue comes from a tree known as Bertholletia excels, originating from the Amazon forest [26, 27]. Over 330 million ha compose the boscages distributed among South American countries. In Brazil, the tree Bertholletia excels has the largest occupied area [26, 27].

The 4-bromophenol (4-BrPhOH) and 4-chloroaniline (4-$ClPhNH_2$) are the emerging contaminants chosen for this study [28]. According to NORMAN, a network of research centers, laboratories, for monitoring of ECs [28], the 4-chloroaniline (4-$ClPhNH_2$) and 4-bromophenol (4-BrPhOH) are listed as the position 488 and 544, respectively, from a list of 1036 emerging contaminants that were cataloged by this research group [28].

4-Chloroaniline is a chemical intermediate primarily employed in the industries of production of pharmaceuticals and drugs, pesticides, and dyes [29]. 4-Chloroaniline is a noxious and hazardous substance that presents some degree of carcinogenicity [29, 30]. It is produced on a large scale; globally, there is potential for human exposure, therefore, characterizing the initiating toxicological event and adverse outcome pathway for tumor development following exposure to 4-chloroaniline is of significant value for human health risk assessments [29, 30].

4-Bromophenol is dispensed in wastewaters of flame retardants, wood preservatives, pesticides, dyes industries [10]. This compound is a non-biodegradable and toxic organic compound [10, 28]. 4-Bromophenol has shown severe impacts on the ecosystem due to its carcinogenic, mutagenic, and genotoxic behavior [10]. Concerns about 4-bromophenol have been increased because of their persistence and bioaccumulation in animals, humans, and plants [10, 28].

This paper aims to study the feasibility of the production of suitable porous-activated carbon from biomass residue for efficient 4-$ClPhNH_2$ and 4-Br-PhOH removal. This research is subdivided into two parts:

1. Production of the porous-activated carbon (AC) from SCP using zinc chloride as the activating agent and following by carbonization in a conventional heating furnace. It is obtained a carbon material with excellent physicochemical properties in terms of porosities and high S_{BET} values. The chemical composition of the activated carbon presents different functional groups that confer hydrophilicity to the material.
2. Application of the produced AC as adsorbent into the removal of 4-$ClPhNH_2$ and 4-Br-PhOH emerging contaminants from aqueous media as well as to test the effectiveness in the treatment of simulated industrial wastewater having many ECs.

2 Materials and methods

2.1 Reagents

The chemical reagents ($ZnCl_2$; HCl, NaOH) used in this study were of analytical grade (Neon, São Paulo, Brazil) and used as received. The emerging contaminants 4-chloroaniline (4-$ClPhNH_2$) and 4-bromophenol (4-BrPhOH) were procured from Acros (New Jersey, USA). The preparation of all solutions was carried out with distilled water. Nitrogen 99.99% was supplied by White Martins (Canoas, Brazil).

2.2 Preparation process of activated carbon

The preparation process of the activated carbon was as following: First, around 90.0 g of the shell of cashew of Para (SCP) was grounded ($\phi < 250$ µm) and blended with 135 g of $ZnCl_2$ dissolved in 70 mL of water. These components were mechanically mixed to form a paste [31]. After drying it at 90 °C for 2 h, the mixture was introduced in a quartz reactor in a ceramic oven. Then, the reactor was heated from 25° up to 700 °C at 10 °C min^{-1} under an N_2 flow rate of 200 mL min^{-1}. The temperature of the furnace was kept fixed at 700 °C for 30 min. Subsequently, the system was chilled under 150 mL min^{-1} of N_2 gas flow until the system attains < 200 °C. To leach-out, the inorganics from the carbonized material, a 1:1 HCl solution was added to a known quantity of the obtained material under reflux (60 min) [31, 32]. The carbon material after the leaching-out was denominated as SCP700.

2.3 Analytical techniques used for characterization

Isotherms of adsorption and desorption of N_2 (at − 196 °C) were recorded by a volumetric analyzer furnished by Micromeritics (TriStar II 3020) for obtaining the superficial area, total pore volume, and pores size distribution. Before running the experiment, the sample was degassed under vacuum at 150 °C. The determination of S_{BET} (specific surface area) was found, as shown elsewhere [33], and the PSD (pore size distribution) was calculated by using the DFT method [34].

The identification of the surface and bulk functional groups of the SCP700 was carried out by FTIR, using an IZ10 Nicolet spectrophotometer [21].

Elemental analysis (CHN/O) was performed with a Thermo Fisher Scientific analyzer (Flash*Smart*) to quantify the proportions (%) of C, H, N, and O in the SCP700 sample [19].

The thermal stability of the SCP700 carbon was studied from 20 to 800 °C under inert nitrogen gas (10 °C min^{-1}), and from 800 to 1000 °C, under oxygen gas. The method used was TGA, and the equipment was analyzer instrument, TA model SDT Q600.[23].

The hydrophobicity/hydrophilicity property (HI) was obtained as recommended elsewhere [17, 21].

Scanning electron microscopy (SEM) analysis of the activated carbon was obtained using a JSM-6610LV Jeol microscope [35].

The pH_{pzc} (point of zero charge) of the adsorbent was obtained as described elsewhere [20, 21]. The total amount (mmol g^{-1}) of basic and acidic groups of the SCP700 carbon was obtained by the Boehm titration method [21, 36].

2.4 Adsorption experiments

The adsorption studies were carried out using the SCP700-activated carbon and 4-BrPhOH and 4-$ClPhNH_2$ as sorbing species [37, 38]. The details about the experiment are found in the supplementary material.

The amount of 4-BrPhOH and 4-$ClPhNH_2$ before and after the adsorption was carried as described elsewhere [39–43].

The nonlinear models were used to fit the experimental data, and the subsequent validation was realized using $R^2_{adjusted}$, the Bayesian information criterion (BIC), and standard deviation (SD) [44, 45]. The further details are explained in the supplementary material.

2.5 Models of kinetic and equilibrium of adsorption

The kinetic adsorption models of Avrami fractional-order, pseudo-first-order, pseudo-second-order were employed to analyze the obtained data.

The equilibrium data were fitted with the Freundlich, Liu, and Langmuir isotherm models. The further details, as well as the equations, are shown the supplementary material [44].

2.6 Thermodynamic studies

The thermodynamic studies were carried out at different temperatures, and the data were analyzed as previously established [44, 46]. The further details, as well as the equations, are given in the supplementary material.

2.7 Synthetic industrial wastewaters

Four synthetic wastewaters containing several inorganic and organic compounds were prepared to study the efficiency of the adsorbent for treating industrial wastewater (Table 1). The composition of organic and inorganic species usually found in industrial wastewaters is shown in Table 1.

Table 1 Composition of the synthetic wastewaters

Wastewater composition	Concentration (mg L^{-1})			
	Effluent 1	Effluent 2	Effluent 3	Effluent 4
Organics				
4-Chloroaniline	45	90	15	30
4-Bromophenol	15	30	45	90
Resorcinol	15	30	15	30
2.4-Diclorophenol	15	30	15	30
4-Nitrophenol	15	30	15	30
Saccharose	30	50	30	50
Glucose	30	50	30	50
Sodium dodecyl sulfate	5	10	5	10
Urea	10	20	10	20
Citric acid	10	20	10	20
Humic acid	10	20	10	20
Inorganic components				
Ammonium chloride	20	30	20	30
Sodium chloride	50	70	50	70
Sodium carbonate	10	20	10	20
Ammonium phosphate	20	30	20	30
Sodium sulfate	10	20	10	20
Sodium carbonate	10	20	10	20
Calcium nitrate	10	20	10	20
Magnesium chloride	10	20	10	20
Potassium nitrate	10	20	10	20
pH*	7.0	7.0	7.0	7.0

3 Results and discussion

3.1 Isotherms of adsorption and desorption of nitrogen

The N_2 adsorption and desorption isotherms of SCP700 is depicted in Fig. 1. SCP700 sample displays the type Ib of isotherm model, according to IUPAC [33]. This isotherm reveals that the SCP700 has pore size distribution incorporate in a broad range composing of pores within 1.0–2.0 nm (wider micropores) and narrow mesopores (< 7.0 nm). This characteristic is adequate for the removal of some contaminants by adsorption process since microporous materials present a remarkable effect on the uptaken of short molecules [32].

The inset of Fig. 1 shows the pore size distribution curve of the SCP700 material obtained using the DFT method [34]. SCP700 does not exhibit micropores < 1 nm. It is possible to see that the SCP700 carbon showed a proportion of micropores in the interval of 1.0–2.0 nm and, also, a considerable proportion of mesopores in the interval of 2–6 nm. Based on this result, SCP700 is a material

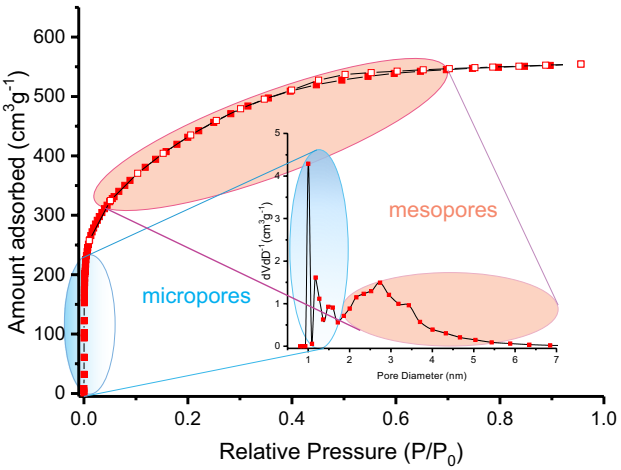

Fig. 1 Textural characteristics of SCP700-activated carbon obtained using the DFT method. Isotherm of adsorption and desorption of N_2; inset curve: pore size distribution curve

with microporous and mesoporous. For pores size < 1 nm, there is no cumulative volume of pores (0.0 g cm^{-3}). From 1 to 2 nm, the cumulative volume of pores is 0.392 g cm^{-3}. From 2 nm up to 31.8 nm (extended scale of the volume of pores, not shown in Fig. 1), the cumulative volume of pores is 0.341 g cm^{-3}. Considering that the total volume of pores is the sum of the volume of pores accumulated in the different regions of pore size distribution [36], the total pore volume of SCP700 is 0.733 g cm^{-3}. From this accumulated gas volume adsorbed, 45.5% is due to the micropores, and 53.5% is due to the volume of mesopores.

The specific surface area (S_{BET}) of SCP700 is 1520 $m^2\ g^{-1}$. Using DFT analysis, the total area of pores is 878 $m^2 g^{-1}$, then the external surface area is 642 $m^2 g^{-1}$. Therefore, the contribution of pores to the total surface area is 57.8%, while the contribution of the external surface for the total area is 42.2%.

Mondal and Majumder [47], performed a procedure of chemical activation of tea wastes using H_3PO_4 as an activating agent, obtaining an activated carbon with an S_{BET} of 1329 $m^2 g^{-1}$ and a total pore volume of 0.417 $cm^3\ g^{-1}$. Bhomick et al. [48] prepared activated carbon from evergreen biomass and chemical activation using KOH. They obtained an activated carbon with an S_{BET} of 1006 $m^2\ g^{-1}$, and a total pore volume of 0.491 $cm^3 g^{-1}$. Although the values of S_{BET} and total pore volume reported by Mondal and Majumder [47] and Bhomick et al. [48], were excellent, the textural characteristics of the obtained SCP700-activated carbon was even better. Therefore, the textural characteristic of SCP700 makes this adsorbent useful for being applied as an adsorbent for the removal of emerging contaminants from aqueous effluents [19, 21, 23].

The $ZnCl_2$, as an activating agent for the preparation of activated carbon, is responsible for the production of ACs with a high surface area [20, 32]. $ZnCl_2$ increases the number of pores on the adsorbent by occupying a space inside the particle of carbon. After leaching-out it from the carbonaceous matrix [31, 32], it generates pores in the carbon structure. With the increase of pores, there is, as a consequence, one increase in the volume of pores, and also, the total superficial area (S_{BET}). This property can utterly improve the active sites on the surface of the material and therefore enhance the 4-BrPhOH and 4-Cl–$PhNH_2$ adsorption. Furthermore, the high porosity of the material favors for the fast diffusion of the emerging contaminants through the pores of the SCP700 material [31, 38].

3.2 Qualitative and quantitative functional groups

Figure 2 shows the FTIR spectra of SCP700. The intense broadband at 3435 cm^{-1} is assigned to OH and N–H group stretching [16, 19]. The two bands at 2922 cm^{-1} and 2852 cm^{-1} are asymmetric and symmetric stretching of C–H groups, respectively [20, 21]. The band at 1747 cm^{-1} is assignable to the C=O of cyclic anhydrides or carbonates [23, 25]; the peak at 1621 cm^{-1} is attributed to C=O stretching of carboxylate [16, 17, 25]. The small peak at 1458 cm^{-1} is attributed to C=C of a ring of aromatic compounds [31, 32]. The small peaks at 1387 and 1317 cm^{-1} are assignable to C–H bond bending or N–C stretching of amides or amines [23, 38]. The band at 1159 cm^{-1} is assigned to stretching of C–C–O of esther or C–O–C of ether [16, 17], and the peak 1045 cm^{-1} is assigned to C–O stretching of carboxylate or phenolic groups [15, 37]. The peak at 815 cm^{-1} is ascribed to the aromatic out-of-plan –CH bending [32].

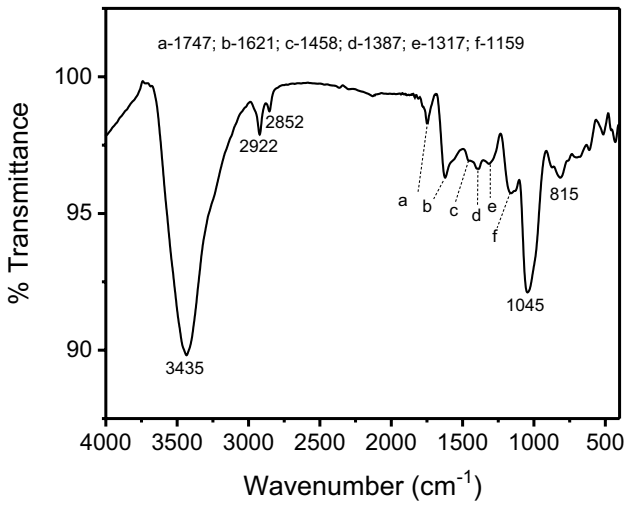

Fig. 2 FTIR spectra of SCP700-activated carbon. Values inside the graph are wavenumber of vibrational bands

From this result, we can observe that the SCP700-activated carbon has a wide variety of surface functional groups that could interact with emerging contaminants during the adsorption experiment by π–π interactions, hydrogen bonds, dispersion interactions, and electron donor–acceptor pair [20, 23].

As a complementarity result of FTIR—which is commonly used for the identification of functional groups on the carbon surfaces—and in bulk, the modified Boehm–titration method was utilized to find the quantities of the total basic and acidic groups present on the surface of the sample [32]. The total amount of acidity and basicity of SCP700-activated carbon was 0.2945 mmol g^{-1} and 0.1369 mmol g^{-1}, respectively (see Table 2). From this result, we can observe that the quantity of acidic groups on the surface of SCP700 was higher than the basic groups—implying that utilizing zinc chloride as an activating agent in the preparation of ACs produces a material with a higher quantity of acidic groups on the SCP700 surface.

When applying the ratio of the total acidic group/total basic group, the value was 2.15, which indicated that the acidic groups were predominant at the carbon surface. The acidic property of the activated carbon is probably due to the presence of acidic groups found previously in the FTIR result (see Fig. 2), such as carboxylates—originally from carboxylic acids. Notwithstanding, the basic properties of activated carbon are generally attributed to the presence of nitrogen-containing groups such as amine and cyclic amides [32]. When we compare the quantity of the total acidic and basic surface functional groups, it is possible to note that the entire basic groups are much lower than the total acidic groups.

Another critical data related to the functional groups on the adsorbent surface is the hydrophobic–hydrophilic Index

Table 2 Elemental analysis, total acidity, and basicity, and hydrophobic Index (HI) of SCP700-activated carbon in comparison with the natural shell of cashew

	Carbon (%)	Hydrogen (%)	Nitrogen (%)	Oxygen (%)	Ash (%)	Total acidity (mmol g^{-1})	Total basicity (mmol g^{-1})	pH_{pzc}	HI
SCP700	79.56	1.25	1.55	17.43	0.22	0.2945	0.1369	5.73	1.006
Shell of cashew	41.52	5.18	0.68	52.62	–	–	–	–	–

(HI) (see Table 2). HI shows the capacity of the material to adsorb nonpolar solvent such as n-heptane or polar solvent such as water, through London dispersive or polar interaction [17, 21]. Depending on the ratio of n-heptane to water adsorption, the material will have a hydrophobic or hydrophilic property [17, 21].

The HI of SCP700-activated carbon was 1.006, corresponding to slightly hydrophobic material, due to the presence of aromatic group and C–H groups present in bulk (see Table 2). Otherwise, SCP700 presents some hydrophilicity that could be attributed to total functional groups (acidic and basic). The groups such as carboxyl (–COOH), carbonyl (C=O), hydroxyl (–OH), amine ($–NH_2$, –NH), and cyclic amides (O=C–NH–) present on the surface of the SCP700 could easily bound with water molecule through hydrogen-bound interaction. These characteristics are significant for the use of such material as an adsorbent in wastewater treatment of the effluents contaminated with emerging contaminants.

3.3 Elemental composition

Table 2 presents the elemental analysis, total basicity, total acidity, and hydrophobic- hydrophilic trend of SCP700 material in comparison with the natural shell of the cashew of Pará. Concerning the elemental analysis of the produced material, it is possible to observe that, initially, the natural shell of cashew exhibited 41.52% in carbon, 5.18% of H-content, and 52.62% of O-content.

However, after the carbonization and leaching processes, the C-content, and N-content increased, respectively, to 79.56% and 1.55%, while the H-content and O-content decreased drastically to 1.25% and 17.43%, respectively. It has been shown [32] that higher C-content implies that the aromatic structure is predominant after the carbonization process. In fact, during the carbonization process, $ZnCl_2$ acts as a dehydrating agent and forms zinc oxides.

The diminution of hydrogen and oxygen amounts is ascribed to the disruption and breaking of weak oxygenated bounds within the structure of the shell of cashew biomass. This fact may lead to a reduction in O-content in the produced activated carbon. The remarkable increase of the nitrogen content can be explained by the fact that nitrogen might not wholly leave the carbonaceous biomass during pyrolysis decomposition, leading to a material slightly rich in nitrogen. This behavior could further be attributed to the fact that zinc chloride selectively took away H and O from the shell of cashew biomass rather than nitrogen and carbon.

3.4 *Point of zero charge (pH_{pzc})*

The pH_{pzc} can be defined as a point where a specific material has zero potential charges on its surface. It is the net surface charges of the material under this point; it is positive, while it is negative above the pH_{pzc} [32].

Figure 3 shows the pH_{pzc} of SCP700-activated carbon. The value of pH_{pzc} of SCP700-activated carbon was 5.73, which falls in the acidic zone. This result suggests that the acidic groups on the surface of the adsorbent are predominant. This result matched with the qualitative and quantitative functional group results, discussed in Sect. 3.3. It is also in agreement with hydrophilic property ascribed to SCP700-activated carbon.

3.5 TGA/DTA analysis and thermal stability of SCP700

The thermal stability of the SCP700 carbon was studied from 20 to 800 °C under inert nitrogen gas (10 °C min^{-1}), and from 800 to 1000 °C, under synthetic air gas, in other to find the ash-content of the activated carbon [49].

Figure 4 exhibits the thermogravimetric curves of the SCP700 material, which can be subdivided into four main sections of weight losses. The first section of weight loss occurring from 22.6 up to 555.2 °C, corresponds to the weight loss of the water bounded in the carbon matrix structure. Only 4.57% weight loss was observed. This loss indicates the high stability of SCP700 carbon, even after the high temperature was applied—which is unusual for the broad application of the material. The second region ranging from 555.2 to 797.2 °C, corresponds to the higher weight losses and can be attributed to the first decomposition of the carbonaceous matrix [32, 49].

Meanwhile, the third region ranging from 797.2 up to 828.3 °C, corresponds to the second significant weight loss and can be attributed to the second decomposition step of the carbonaceous matrix. The percentages of the weight losses

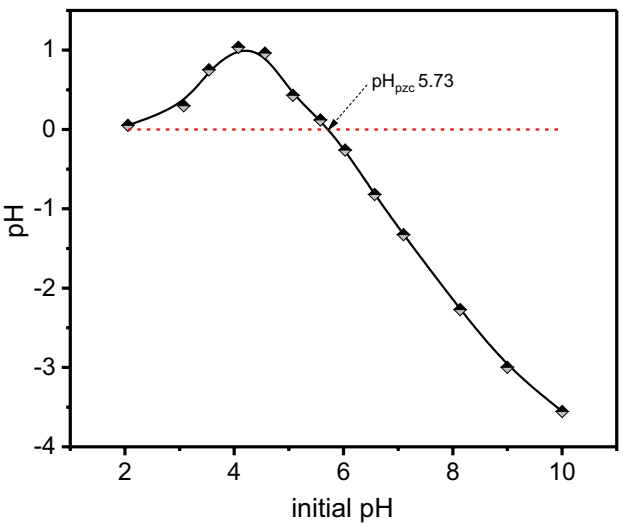

Fig. 3 Point of zero charge of SCP700 carbon

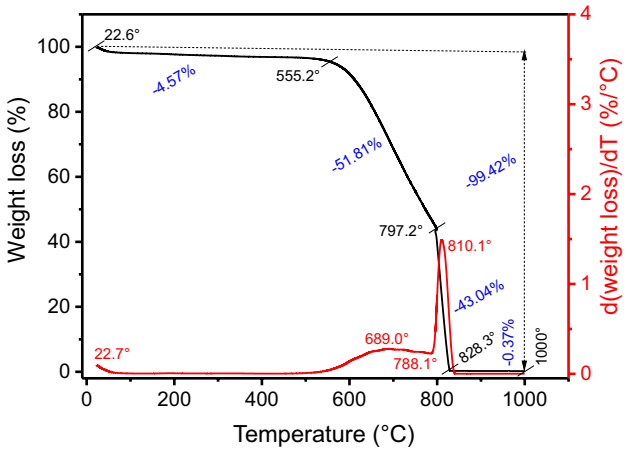

Fig. 4 TGA and DTG curves of SCP700 carbon

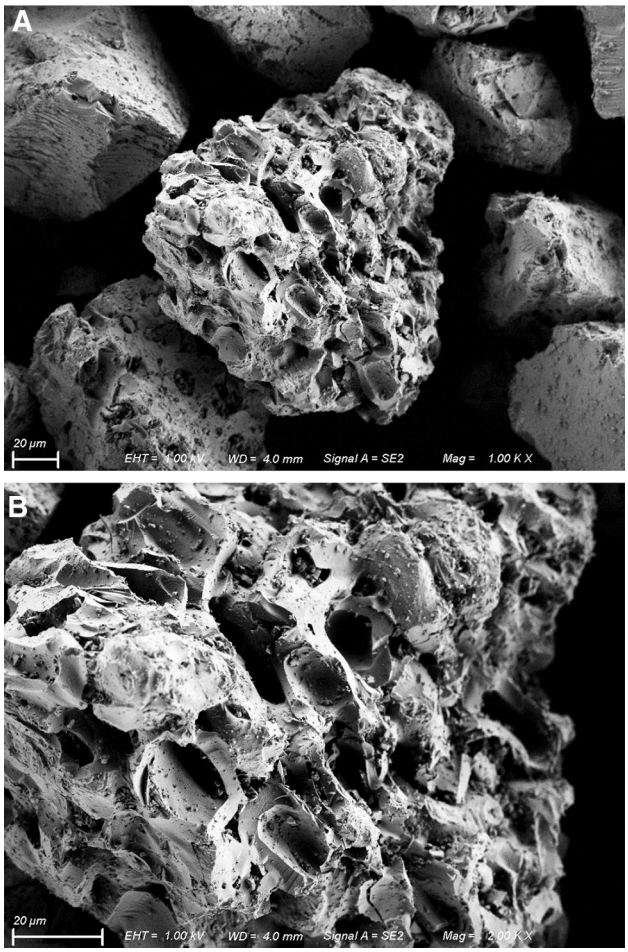

Fig. 5 SEM images of SCP700 carbon with a magnification of × 1000 (**a**) and magnification of × 2000 (**b**)

in the second and third stages of weight loss were 51.81 and 43.04%, respectively. After the third stage of weight loss, most volatile organic compounds are eliminated. The last section ranging from 828.3 up to 1000 °C, is attributed to the skeleton decomposition under the synthetic air atmosphere. The overall weight loss was 94.85%. The remaining residual mass at 1000 °C (0.37%) was inorganic ash of the SCP700 carbon.

3.6 Surface morphology of SCP700

The surface image was *of* SCP700-activated carbon was analyzed by Scanning Electron microscopy (SEM). Figure 5 exhibits SEM images of SCP700 carbon with a magnification of 1000× (a) and magnification of 2000× (b). The images exhibit a material with high rugosity at the surface, with tiny and heterogeneous holes, which is compatible with the presence of channels for solvent passage. These characteristics can be related to the stronger influence of zinc chloride on the shell of cashew material, as we discussed in our previous study [32, 49].

3.7 *Preliminary experiments of adsorption of 4-ClPhNH$_2$ and 4-BrPhOH onto SCP700 carbon and its kinetic studies*

Experiments varying the initial pH of 4-ClPhNH$_2$ and 4-BrPhOH were carried out from an initial pH of 2.0–10.0 onto SCP700-activated carbon. The results are depicted in Supplementary Fig. 3. For 4-ClPhNH$_2$, the sorption was practically constant from pH 4.0 to 10.0 (Supplementary Fig. 3a), and for 4-BrPhOH, the sorption capacity did not change drastically from pH 2.0 to 8.5 (Supplementary Fig. 3b). 4-ClPhNH$_2$ presents pK$_a$ 3.49 (see Supplementary Fig. 2). At high acidic pH solutions occur in the following reaction:

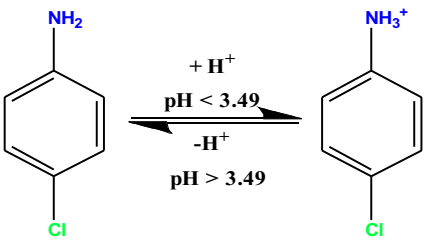

(1)

The protonated specie is a cation that is more soluble than the nonionic specie. As seen in Supplementary Fig. 3, the sorption capacity is lower when the cationic specie is formed, due to the competition of the cationic specie for the carbon surface and water. For further experiments, the pH of 4-ClPhNH$_2$ was fixed at 7.0. On the other hand, for 4-BrPhOH, the sorption capacity decreased from pH 8.5 to 10.0. At alkaline medium (pKa of 4-BrPhOH is 9.09, see Supplementary Fig. 1), the 4-BrPhOH loses a proton, forming an anionic specie as depicted below:

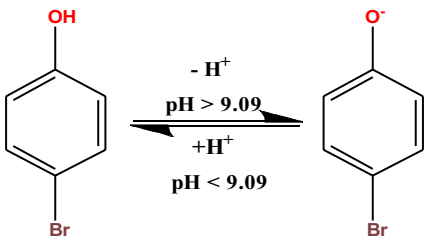

(2)

The solubility of the anionic specie in water is drastically increased at pH > 9.09; therefore, there is a competition of the anionic specie between the carbon surface of SCP700 and the water. This behavior explains the drop in sorption capacity. In further experiments, the initial pH of 4-BrPhOH was fixed at 7.0.

The kinetic studies of 4-BrPhOH and 4-ClPhNH$_2$ adsorption onto SCP700 carbon were explored using three nonlinear kinetic models: pseudo-first-order, pseudo-second-order, and Avrami fractional-order. The fitting parameters of the models and kinetic curves are shown in Table 3 and Fig. 6, respectively.

The results showed that the adsorption process was rapid and reached the equilibrium in the first 10 min when the concentration of both 4-BrPhOH and 4-ClPhNH$_2$ solutions was 500 mg L^{-1}. When double the concentration (1000 mg L^{-1}), no significant changes were observed on the equilibrium time. Therefore, the concentration in this study does not affect the equilibrium time.

Considering the SD, $R^2_{adjusted}$, and the BIC values of the three kinetic models used to fit experimental data, the Avrami fractional-order appeared as the best one, which described the adsorption phenomena. The best-fitted model is the one that presents R^2_{adj} closer to 1.000, lower values of SD, and lower values of BIC. The R^2_{adj} were 0.9995 and 0.9997 for 4-BrPhOH and 0.9995 and 0.9999 for 4-ClPhNH$_2$, respectively, at 500 mg L^{-1} and 1000 mg L^{-1}, for the Avrami fractional-order model. On the other hand, the SD values were 1.925 mg g^{-1} and 0.7173 for 4-BrPhOH and 0.5973 and 0.2704 mg g^{-1} for 4-ClPhNH$_2$, respectively, at 500 mg L^{-1} and 1000 mg L^{-1}. These values were lower and almost close to zero compared to the two other kinetic models. The same trend was observed with the Bayesian information criterion (BIC) values, which are lower for the Avrami fractional-order model compared to the two other models. When the difference of BIC values is higher than 10, it means that the model with lower BIC values is certainly the best-fitted model [45]. The differences between BIC values of Avrami fractional-order and pseudo-first-order were within 27.9–71.6, and for Avrami fractional-order and pseudo-second-order were within 44.5–114.6. These so significant differences of BIC values guarantee that Avrami fractional-order indeed explains the kinetics of adsorption of both adsorbates on the chosen adsorbent.

Table 3 Kinetic parameters of Avrami fractional-order, pseudo-first-order, and pseudo-second-order adsorption of 4-ClPhNH$_2$ and 4-BrPhOH onto SCP700 carbon

C_0 (mg L^{-1})	4-BrPhOH		4-ClPhNH$_2$	
	500.0	1000.0	500.0	1000.0
Avrami fractional-order				
q_e (mg g^{-1})	322.6	454.8	317.5	475.4
k_{AV} (min^{-1})	0.6358	0.6592	0.4257	0.4263
n_{AV}	0.7776	0.7041	1.153	1.185
$t_{1/2}$ (min)	0.9817	0.9031	1.709	1.722
$t_{0.95}$ (min)	6.449	7.207	6.084	5.922
R^2 adjusted	0.9995	0.9997	0.9995	0.9999
SD (mg g^{-1})	1.925	0.7173	0.5973	0.2704
BIC	30.31	35.79	31.01	4.165
Pseudo-first order				
q_e (mg g^{-1})	320.6	450.6	318.4	477.04
k_1 (min^{-1})	0.6038	0.6131	0.4292	0.4297
$t_{1/2}$ (min)	1.148	1.130	1.615	1.613
$t_{0.95}$ (min)	4.961	4.886	6.979	6.972
R^2_{adj}	0.9937	0.9890	0.9974	0.9969
SD (mg g^{-1})	1.972	3.742	1.417	2.327
BIC	71.12	92.01	58.91	75.78
Pseudo-second order				
q_e (mg g^{-1})	329.9	463.7	329.7	494.1
k_2 (g mg^{-1} min^{-1})	0.003570	0.002560	0.002220	0.001480
$t_{1/2}$ (min)	0.8494	0.8403	1.365	1.369
$t_{0.95}$ (min)	16.14	15.97	25.94	26.03
R^2_{adj}	0.9896	0.9945	0.9634	0.9613
SD (mg g^{-1})	2.842	2.889	6.0547	9.359
BIC	79.74	80.33	104.0	118.8

Conditions: pH 7.0; m = 30 mg; temperature = 25 °C

The $t_{0.95}$ (min), which is the time where 95% of the saturation was achieved, were 6.449 and 7.207 min for 4-BrPhOH and 6.084 and 5.922 min for 4-ClPhNH$_2$, respectively, at 500 mg L^{-1} and 1000 mg L^{-1}, for the Avrami fractional-order model. This time shows that both 4-BrPhOH and 4-ClPhNH$_2$ molecules adsorbed very quickly onto SCP700 carbon. At the initial concentration of 500 mg L^{-1}, no significant difference was observed for the adsorbed amount. Notwithstanding, it is possible to observe the difference in the adsorption capacity (q_e). 4-ClPhNH$_2$ showed a relatively high adsorbed amount (475.4 mg g^{-1}) compared to 4-BrPhOH (317.5 mg g^{-1}) when the solution had an initial concentration of 1000 mg L^{-1} (Table 3). The $t_{0.5}$ (min), which is the time where 50% of the saturation was achieved, was also analyzed. The $t_{0.5}$ (min) was less than 1 min for 4-BrPhOH and less than 2 min for 4-ClPhNH$_2$ (see Table 3). The further experiments were carried at the equilibrium time > 10 min for a convenient perspective and to ensure the whole interaction

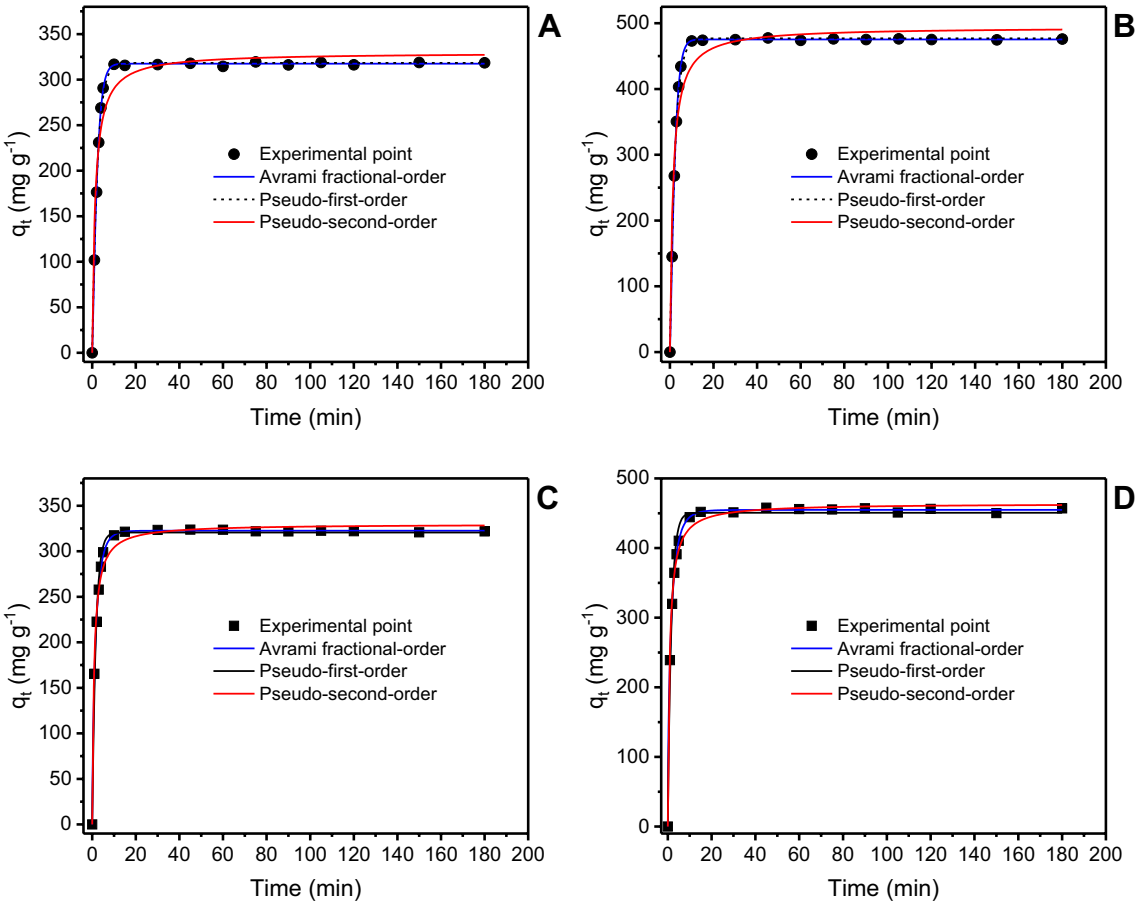

Fig. 6 Kinetics curves of adsorption of 4-ClPhNH$_2$ and 4-BrPhOH onto SCP700 carbon. **a** 500 mg L^{-1} of 4-ClPhNH$_2$; **b** 1000 mg L^{-1} of 4-ClPhNH$_2$; **c** 500 mg L^{-1} of 4-BrPhOH; **d** 1000 mg L^{-1} of 4-BrPhOH. The temperature was fixed at 25 °C, adsorbent dosage 1.5 g L^{-1}, initial pH of 7.0

between emerging organic contaminants and SCP700 adsorbent.

3.8 *Isotherm studies of 4-BrPhOH and 4-ClPhNH$_2$ adsorption onto SCP700 carbon*

The isotherm study gives information about the relationship between 4-BrPhOH and 4-ClPhNH$_2$ adsorbed onto the SCP700 carbon phase and the amounts of adsorbates in the solution when the adsorption process reached the equilibrium [31]. The fitted parameters of the three models are shown in Table 4.

The experimental procedure of the isotherms data was carried out varying temperatures between 10 and 45 °C, initial pH of 4-BrPhOH, and 4-ClPhNH$_2$ solutions was 7.0, and adsorbent dosage was 1.5 g L^{-1}; and the time of contact between the sorbing specie and the adsorbent of 30 min. Figure 7 shows the isotherms of adsorption of 4-ClPhNH$_2$ and 4-BrPhOH at 25 °C. Table 4 shows the fitting parameters of 4-BrPhOH and 4-ClPhNH$_2$ adsorption isotherm onto SCP700 carbon at various temperatures.

Based on SD values, BIC values, and R^2_{adj}, Liu's model was the most suitable for describing the equilibrium data of adsorption of both 4-BrPhOH and 4-ClPhNH$_2$ onto SCP700 carbon at all temperatures (see Table 4).

The Liu model showed the lowest SD values that mean that their theoretical q_e values are closer to those experimentally found q_e (see Table 4). For 4-BrPhOH, the SD values of the Liu model ranged from 0.2800 to 1.236 mg g^{-1}, while for Langmuir ranged from 4.519 to 8.582 mg g^{-1}, and Freundlich from 13.23 to 20.23 mg g^{-1}. For 4-ClPhNH$_2$ adsorbate, the SD values of the Liu model ranged from 0.1036 to 0.3465 mg g^{-1}, while ranged from 0.3918 to 11.53 mg g^{-1} and from 15.45 to 40.05 mg g^{-1} for Langmuir and Freundlich respectively. These data are also supported by the R^2_{adj}, which was almost 1.000 for both molecules at all temperatures.

The BIC values match with the SD values and the R^2_{adj}, strengthening the arguments for the suitability of the Liu

Table 4 Adsorption parameters of the Liu, Freundlich, and Langmuir isotherm models for the removal of 4-ClPhNH$_2$ and 4-BrPhOH onto SCP700 carbon

	10 °C	20 °C	25 °C	30 °C	40 °C	45 °C
4-BrPhOH						
Langmuir						
Q_{max} (mg g^{-1})	421.6	455.0	457.6	430.5	447.9	457.9
K_L (L mg^{-1})	0.4156	0.2663	0.2229	0.2299	0.1536	0.1258
R^2_{adj}	0.9591	0.9888	0.9918	0.9728	0.9859	0.9895
SD (mg g^{-1})	8.582	5.380	4.519	7.201	5.986	5.822
BIC	103.5	88.17	82.13	97.92	90.30	87.07
Freundlich						
K_F (mg g^{-1} (mg L^{-1})$^{-1/nF}$)	222.7	214.4	211.5	200.9	182.1	172.1
n_F	8.499	7.671	7.461	7.485	6.377	5.949
R^2_{adj}	0.9622	0.9180	0.9396	0.9663	0.9483	0.9449
SD (mg g^{-1})	13.23	20.23	16.981	13.45	16.85	15.83
BIC	102.33	117.99	112.3	101.1	109.8	111.9
Liu						
Q_{max} (mg g^{-1})	473.8	476.5	477.9	482.5	483.2	488.2
K_g (L mg^{-1})	0.3467	0.2495	0.2113	0.1799	0.1306	0.1111
n_L	0.4950	0.7037	0.7266	0.5344	0.6636	0.7075
R^2_{adj}	1.0000	0.9999	0.9999	0.9999	0.9999	0.9999
SD (mg g^{-1})	0.6571	0.2800	0.3077	1.236	0.3428	0.5796
BIC	− 12.50	− 19.35	− 19.15	2.939	− 25.92	− 7.784
4-ClPhNH$_2$						
Langmuir						
Q_{max} (mg g^{-1})	449.8	452.0	489.9	526.5	556.2	553.8
K_L (L mg^{-1})	0.2629	0.2126	0.1730	0.1659	0.1575	0.1018
R^2_{adj}	0.9911	0.9832	0.9968	0.9969	0.9502	0.9999
SD (mg g^{-1})	3.349	4.752	2.328	2.782	11.53	0.3918
BIC	88.73	100.2	73.63	78.75	125.9	10.44
Freundlich						
K_F (mg g^{-1} (mg L^{-1})$^{-1/nF}$)	267.8	247.1	278.6	275.8	322.8	223.1
n_F	12.034	10.188	11.048	9.471	11.546	6.893
R^2_{adj}	0.9491	0.9570	0.9369	0.8407	0.8046	0.8565
SD (mg g^{-1})	16.61	15.45	19.51	32.77	40.05	31.34
BIC	118.3	116.2	124.6	145.7	149.2	148.9
Liu						
Q_{max} (mg g^{-1})	464.9	481.9	499.6	518.2	534.8	552.5
K_g (L mg^{-1})	0.2958	0.2165	0.1863	0.1629	0.1200	0.1022
n_L	0.6909	0.6022	0.8154	1.1976	2.292	1.0180
R^2_{adj}	0.9999	0.9999	0.9999	0.9999	0.9999	0.9999
SD (mg g^{-1})	0.2819	0.3465	0.2349	0.1046	0.1036	0.2047
BIC	− 17.72	− 23.76	− 20.72	− 35.92	− 28.65	− 19.51

Conditions: $m = 30$ mg, and initial pH 7.0, time of contact of 30 min

model for 4-chloroaniline (4-ClPhNH$_2$) and 4-bromophenol (4-BrPhOH) adsorption onto SCP700 material. The BIC is commonly used to compare different models with different numbers of parameters. When the difference of BIC values is > 10 [45], the model having the lowest BIC value is the best model to be chosen. From Table 4, it is possible to see that the ΔBIC values between Liu model and Langmuir and Liu model and Freundlich model were always higher than 10 for both 4-chloroaniline (4-ClPhNH$_2$) and 4-bromophenol (4-BrPhOH). It is worth to notice that all the BIC values of the Langmuir and Freundlich models were positive, ranging from 82.13 to 103.5 and 101.1 to 117.99, respectively, for 4-BrPhOH, and from 10.44 to 125.9 and 116.2 to 149.2, respectively, for 4-ClPhNH$_2$ (see Table 4). Notwithstanding, all the BIC values of Liu's model were negative for both molecules.

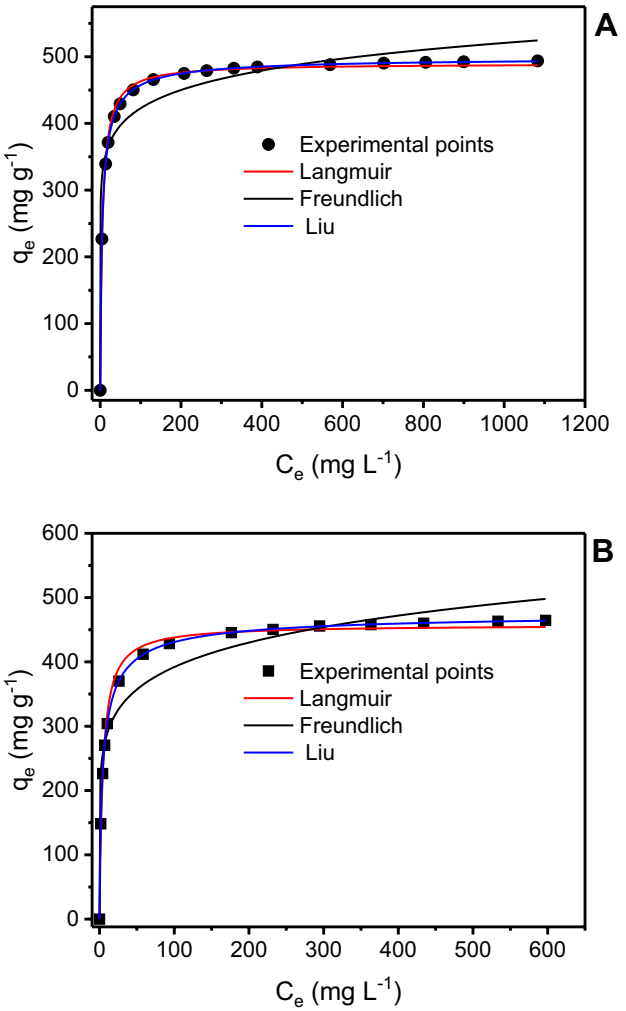

Fig. 7 Isotherms of adsorption of 4-ClPhNH$_2$ and 4-BrPhOH onto SCP700 carbon at 25 °C. **a** 4-ClPhNH$_2$; **b** 4-BrPhOH. Conditions adsorbent mass of 30 mg; initial pH 7.0. Time of contact of 30 min

It is crucial to notice that the adsorption capacity (Q_{max}) of both adsorbates was increased as the temperature also increased. When varying the temperature from 10 to 45 °C, the Q_{max} values increased from 473.8 to 488.2 mg g^{-1} and from 464.9 to 552.5 mg g^{-1}, respectively, for 4-BrPhOH and 4-ClPhNH$_2$. However, it is possible to observe the difference in adsorption capacity (Q_{max}). As previously discussed in Sect. 3.7, 4-ClPhNH$_2$ shows a relatively high adsorbed amount compared to 4-BrPhOH when the temperature increased, due probably to the possible more interaction with surface functional groups of the adsorbent.

3.9 Adsorption thermodynamics

Adsorption thermodynamics is a crucial tool to deduce whether the adsorption process is spontaneous or not. For that purpose, both entropy and energy variations should be taken into account. Calculations of the thermodynamic parameters were by the plot of Ln(K) versus *1/T*, allowing to obtain $\Delta S°$ and $\Delta H°$ values, respectively [46].

The changes in Gibbs free energy ($\Delta G°$) and enthalpy ($\Delta H°$) for the increase in temperature is an essential indicator to justify whether the adsorption of 4-ClPhNH$_2$ and 4-BrPhOH onto SCP700 carbon was spontaneous and had an exothermic or endothermic nature, respectively [49, 50].

To infer the abovementioned thermodynamic adsorption parameters of 4-ClPhNH$_2$ and 4-BrPhOH onto SCP700 carbon, experiments were carried out at different temperatures from 283 to 318 K (10–45 °C), and the values are reported in Table 5. More details about the calculation method of the parameters are found in the supplementary material.

The $\Delta G°$ and $\Delta H°$ in this study are all negative (see Table 5). These results suggest a spontaneous and exothermic adsorption process, respectively. All enthalpy values were $\Delta H° < -25$ kJ mol^{-1}. According to Chang and Thoman [51], the magnitude of enthalpy matches with physical adsorption. Furthermore, the positive values of the entropy

Table 5 Thermodynamic parameters of the adsorption of 4-ClPhNH$_2$ and 4-BrPhOH onto SCP700 carbon

Temperature (K)	283	293	298	303	313	318
4-BrPhOH						
K_g (L mol^{-1})	59,976	43,167	36,558	31,122	22,601	19,219
$\Delta G°$ (kJ mol^{-1})	−25.89	−25.99	−26.03	−26.06	−26.09	−26.08
$\Delta H°$ (kJ mol^{-1})	–	–	−24.36	–	–	–
$\Delta S°$ (J K^{-1} mol^{-1})	–	–	5.520	–	–	–
R^2_{adj}	–	–	0.9989	–	–	–
4-ClPhNH$_2$						
K_g (L mol^{-1})	37,746	27,624	23,766	20,786	15,313	13,031
$\Delta G°$ (kJ mol^{-1})	−24.80	−24.91	−24.96	−25.05	−25.08	−25.05
$\Delta H°$ (kJ mol^{-1})	–	–	−22.60	–	–	–
$\Delta S°$ (J K^{-1} mol^{-1})	–	–	7.890	–	–	–
R^2_{adj}	–	–	0.9980	–	–	–

($\Delta S°$) indicate that an increase in randomness occurs during the adsorption process of 4-ClPhNH$_2$ and 4-BrPhOH onto SCP700 material, at the adsorbent/liquid interface [49]. This behavior should be explained by the releases of hydration water of both 4-ClPhNH$_2$ and 4-Br-PhOH before these molecules arriving at the active site of the adsorbent [49]. The R^2_{adj} values of the plots are 0.9980 and 0.9989, respectively. These values show the high reliability of the $\Delta H°$, and $\Delta S°$ values obtained.

3.10 Adsorption mechanism

Based on the abovementioned thermodynamic parameters and the results from the physicochemical characterization of the AC, we can propose the adsorption mechanism of 4-ClPhNH$_2$ and 4-BrPhOH onto SCP700 material.

The enthalpy data show that the interaction between both 4-ClPhNH$_2$ and 4-BrPhOH and SCP700 was physical. In that sense, the possible interactions are π–π interactions, hydrogen bonds, electron donor–acceptor, and dispersion interactions [21, 50]. In fact, at the surface of SCP700 carbon, several functional groups are present such as, –COO, –OH, and –NH, (see Fig. 2) and might interact with the N–H and –O–H group of 4-ClPhNH$_2$ and 4-BrPhOH molecules, forming hydrogen bonds [21].

The adsorption of 4-ClPhNH$_2$ and 4-BrPhOH on AC can further occur by π–π interactions. Indeed, the π electrons moving inside the aromatic ring in the 4-ClPhNH$_2$ and 4-BrPhOH structure, as shown in supplementary Figs. 1 and 2, might react with the π electrons of the aromatic rings of the SCP700 carbon. The formation of the pair donor–acceptor can occur between the aromatic ring of 4-ClPhNH$_2$ and 4-BrPhOH, acting as the electron acceptor and the carbonyl groups (electron donors) present at the SCP700 surface.

According to Lipkowski et al. [52], it is also possible to find pure acid–base hydrogen bond interactions of –COOH or –OH of AC with Cl (O–H–Cl) or Br (O–H–Br) of 4-ClPhNH$_2$ and 4-BrPhOH, respectively. Notwithstanding, the pore structure of the material can also cause adsorption by pore filling. As discussed in Sect. 3.1, the textural characteristics of the SCP700 can utterly improve the active sites on the surface of the material and therefore enhance the 4-BrPhOH and 4-Cl-PhNH$_2$ uptaken. The high porosity of the material favors the quick inter-diffusion of the 4-ClPhNH$_2$ and 4-BrPhOH molecules, which might be seized in those pores.

3.11 Application treatment of a simulated effluent

To evaluate the effectiveness of the produced activated carbon from Brazil nutshells biomass in the real industrial wastewater treatment plants, a simulated effluent was prepared and tested with SCP700 carbon. The synthetic wastewaters are made with many other contaminants classified as emerging contaminants, and several other chemical compounds that are usually detected in industrial wastewaters. The chemical compositions of the synthetic wastewaters used for the experiment in this study are shown in Table 1. Four effluents were prepared with a mixture of other pharmaceuticals and phenols molecules.

The UV–Vis spectra of the four simulated effluents before and after adsorption (190–450 nm) experiment were recorded and used to find the quantities of the emerging contaminants from effluents that were removed (Fig. 8). The total absorbance of a mixed solution at any wavelength is equal to the sum of the absorbances of the individual components in the solution [53], because absorbance is an additive property [53]. Therefore, the integration of the area under the absorption peak (190–450 nm) will correspond to the sum of the concentration of all the substances depicted in Table 1. When we make the integration of the areas of absorption bands from 190 to 450 nm of the simulated effluents before and after the treatment, and also the ratio of the area of the treated synthetic wastewater divided by the area of untreated one and multiplying this values by 100, it is possible to find the percentage of total removal of the organic compounds from the simulated effluents [50].

The results show that the percentage of the removal was 98.64%, 98.25%, 98.60%, and 97.92%, respectively, for the effluent 1, 2, 3 and 4. It is crucial to notice that SCP700 carbon still showed a high percentage of removal of organic compounds even when doubling the concentration of the pollutants and other chemicals, which is the case for effluent 2 and effluent 4. These findings indicate that SCP700-activated carbon from the cashew of the Para shell could be used with effectiveness for the real wastewater treatment plants.

It is relevant to highlight that in all spectra in Fig. 8 after the adsorption, the spectra of the organics (190–250 nm) were not zero; however, before the treatment, the spectra of the initial effluent were diluted 10× (effluents 1 and 3) and 20× (effluents 2 and 4).

3.12 *Comparison of the adsorption capacity of 4-ClPhNH$_2$ and 4-BrPhOH molecules onto SCP700-activated carbon with other materials*

Table 6 below presents the adsorption capacity of 4-ClPhNH$_2$ and 4-BrPhOH molecules onto SCP700-activated carbon with other materials reported in the literature under the same conditions. We also reported the comparison with other contaminants such as 4-chlorophenol and aniline. It appears that SCP700-activated carbons prepared in this work have a significant adsorption capacity for both adsorbates compared to other adsorbents and contaminants, which is mentioned in Table 6. SCP700-activated carbons

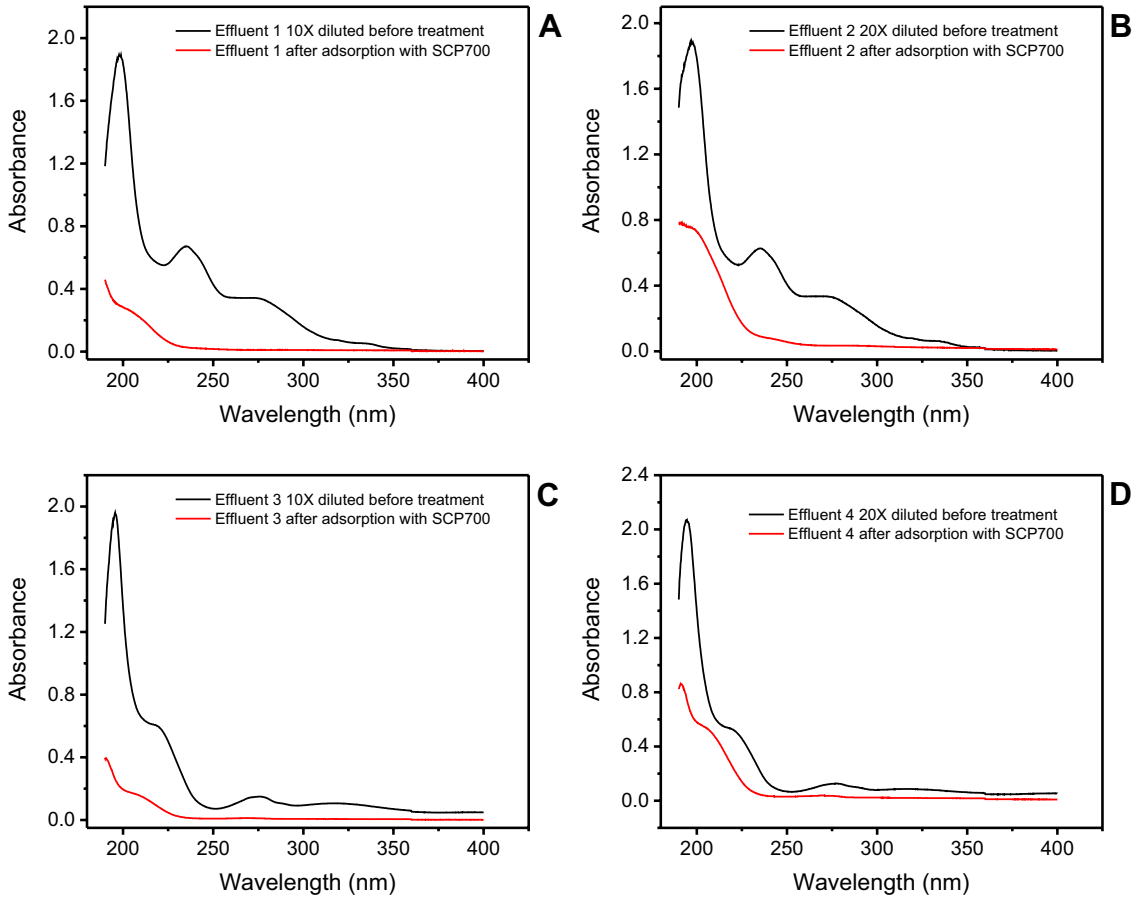

Fig. 8 UV/Vis spectra of simulated industrial effluents before and after treatment with SCP700 activated carbon. **a** Effluent 1; **b** effluent 2; **c** effluent 3; **d** effluent 4. See Table 1 for the composition of effluents

Table 6 Comparison of the adsorption capacities for the uptake of chlorophenols, bromophenols, and anilines molecules onto different adsorbents materials

Adsorbates	Adsorbents	Maximum adsorption capacity (Q_{max}; mg g^{-1})	References
4-Chlorophenol	Functionalized magnetic MCM-48 nanoporous silica by cyanuric chloride	239.55	[54]
4-Bromophenol		222.9	[54]
4-Chlorophenol	Biosolid biochar	47.7	[55]
4-Bromophenol	Biosolid biochar	47.2	[55]
4-Chlorophenol	Activated carbon (GAC)	203	[55]
4-Bromophenol	Activated carbon (GAC)	171	[55]
4-Chlorophenol	Polymer/RS-derived biochar pyrolyzed at 550 °C	9.2	[56]
Aniline	Activated kaolinite	109	[57]
4-Chloroaniline	Multiwalled carbon nanotubes	100	[58]
4-$ClPhNH_2$	SCP700-activated carbon	552.5	This work
4-BrPhOH	SCP700-activated carbon	488.2	This Work

exhibit higher adsorption density compared to Functionalized magnetic MCM-48 nanoporous silica by cyanuric [54], biosolid biochar [54], activated carbon (GAC) [55], polymer/RS-derived biochar pyrolyzed at 550 °C [56], activated kaolinite [57] and multiwalled carbon nanotubes [58]. SCP700-activated carbons adsorbed more than two times of 4-BrPhOH molecule compared to Functionalized magnetic MCM-48 nanoporous silica by cyanuric chloride, reported in Table 6 as the best adsorbent. Furthermore, the Q_{max} obtained for 4-$ClPhNH_2$ was five times higher than

the adsorption capacity of aniline, five and half times than the Multiwalled Carbon Nanotubes, and almost two times higher than the adsorption of 4-chlorophenol for the best adsorbent reported here. This result shows that SCP700-activated carbons prepared in this study can be potentially used in the treatment of wastewater contaminated with emerging contaminants.

4 Conclusion

In this study, activated carbon from the shell of the cashew of Para (SCP) was produced by chemical activation with $ZnCl_2$ using the ratio of SCP: $ZnCl_2$ 1.0:1.5 at 700 °C. The prepared activated carbon (SCP700) was used in the removal of two emerging contaminants, 4-bromophenol (4-BrPhOH) and 4-chloroaniline (4-$ClPhNH_2$) that are primarily employed in the industry.

Different analytical techniques characterized the produced material. The N_2 adsorption–desorption isotherms presented the specific surface area of 1520 $m^2\ g^{-1}$ and total pore volume of 0.492 $cm^3\ g^{-1}$. The functional groups were identified by the FTIR technique and quantified by modified Boehm titration. The results revealed the presence of different functional groups on the SCP700 surface, which can utterly affect the removal of the emerging contaminants.

The equilibrium experiments showed that the maximum uptaken capacities (Q_{max}) achieved at 45 °C were 488.2 (4-BrPhOH) and 552.5 mg g^{-1} (4-$ClPhNH_2$). The thermodynamic assessments revealed that the process of 4-BrPhOH and 4-$ClPhNH_2$ adsorption are spontaneous and exothermic, and the magnitude of $\Delta H°$ is matching with a physical adsorption process.

The mechanism of adsorption of both adsorbates onto the carbon surface is dominated by microporous filling, hydrogen bonds, π-stacking interactions, and other Van der Waals interactions. The use of activated carbon for the treatment of synthetic wastewaters containing inorganic and organic compounds exhibited a high percentage of uptaken (up to 98.64%). These findings indicate that SCP700-activated carbon from the shell of the cashew of Para could be used with effectiveness for the real wastewater treatment plants.

Acknowledgements The authors thank the Foundation for Research Support of the State of Rio Grande do Sul (FAPERGS), National Council for Scientific and Technological Development (CNPq, Brazil), and Coordination of Improvement of Higher Education Personnel (CAPES, Brazil) (Grand Number 2018) for financial support and sponsorship. Dr. Pascal Silas Thue is grateful to the CAPES for the postdoctoral scholarship granted through the National Postdoctoral Program (PNPD). Authors are grateful to Nanoscience and Nanotechnology Center (CNANO-UFRGS), and Microscopy and Microanalysis Center (CME-UFRGS) of Federal University of Rio Grande do Sul (UFRGS). We are also grateful to ChemAxon for giving us an academic research license for the Marvin Sketch software, Version 20.3. (https://www.chemaxon.com), 2020 used for molecule physical–chemical properties.

References

1. Rodriguez-Narvaez OM, Peralta-Hernandez JM, Goonetilleke A, Bandala ER (2017) Treatment technologies for emerging contaminants in water: a review. Chem Eng J 323:361–380
2. Sophia CA, Lima EC (2018) Removal of emerging contaminants from the environment by adsorption. Ecotoxicol Environ Saf 150:1–17
3. Grassi M, Kaykioglu G, Belgiorno V, Lofrano G (2012) Chapter 2-removal of emerging contaminants from water and wastewater by adsorption process, in emerging compounds removal from wastewater. In: G. Lofrano (ed) Springer briefs in green chemistry for sustainability. Belgiorno, Lofrano. https://doi.org/10.1007/978-94-007-3916-1_2
4. Taheran M, Naghdi M, Brar SK, Verma M, Surampalli RY (2018) Emerging contaminants: here today, there tomorrow! Environ Nanotech Monit Manage 10:122–126
5. Ebele AJ, Abdallah MAE, Harrad S (2017) Pharmaceuticals, and personal care products (PPCPs) in the freshwater aquatic environment. Emerg Contam 3:1–16
6. Silva B, Costa F, Neves IC, Tavares T (2015) Psychiatric pharmaceuticals as emerging contaminants in wastewater. Springer, Cham. https://doi.org/10.1007/978-3-319-20493-2
7. Rizzo L, Malato S, Antakyali D, Beretsou VG, Đolić MB, Gernjak W, Heath E, Ivancev-Tumbas I, Karaolia P, Ribeiro ARL, Mascolo GL, McArdell CS, Schaar H, Silva AMT, Fatta-Kassinos D (2019) Consolidated vs. new advanced treatment methods for the removal of contaminants of emerging concern from urban wastewater (Review). Sci Total Environ 655:986–1008
8. Kanaujiya DK, Paul T, Sinharoy A, Pakshirajan K (2019) Biological treatment processes for the removal of organic micropollutants from wastewater: a review. Curr Pollut Rep 5:112–128
9. Sutherland DL, Ralph PJ (2019) Microalgal bioremediation of emerging contaminants—opportunities and challenges. Water Res 164:114921. https://doi.org/10.1016/j.watres.2019.114921
10. Naraginti S, Yong YC (2019) Enhanced detoxification of p-bromophenol by novel Zr/Ag-TiO_2@rGO ternary composite: degradation kinetics and phytotoxicity evolution studies. Ecotox Environ Saf 170:355–362
11. Wang Y, Yu G, Deng S, Huang J, Wang B (2018) The electroperoxone process for the abatement of emerging contaminants: mechanisms, recent advances, and prospects. Chemosphere 208:640–654
12. Serna-Galvis EA, Botero-Coy AM, Martínez-Pachón D, Moncayo-Lasso A, Ibáñez M, Hernández F, Torres-Palma RA (2019) Degradation of seventeen contaminants of emerging concern in municipal wastewater effluents by sonochemical advanced oxidation processes. Water Res 154:349–360
13. Teodosiu C, Gilca AF, Barjoveanu G, Fiore S (2018) Review Emerging pollutants removal through advanced drinking water treatment: a review on processes and environmental performance assessment. J Clean Prod 197:1210–1221
14. Cristóvão MB, Torrejais J, Janssens R, Luis P, Van der Bruggen B, Dubey KK, Mandal MK, Bronze MR, Crespo JG, Pereira VJ (2019) Treatment of anticancer drugs in hospital and wastewater effluents using nanofiltration. Sep Purif Technol 224:273–280
15. Sun L, Shi P, Zhang Q, Lv J, Zhang Y (2019) Effects of using different ultrafiltration membranes on the removal efficiency of antibiotic resistance genes from secondary effluent. Desalin Water Treat 156:52–58

16. Rovani S, Censi MT, Pedrotti SL Jr, Lima EC, Cataluña R, Fernandes AN (2014) Development of a new adsorbent from agro-1 industrial waste and its potential use in endocrine disruptor compound removal. J Hazard Mater 271:311–320
17. dos Reis GS, Sampaio CH, Lima EC, Wilhelm M (2016) Preparation of novel adsorbents based on combinations of polysiloxanes and sewage sludge to remove pharmaceuticals from aqueous solutions. Colloid Surf A Physicochem Eng Aspects 497:304–315
18. Sophia AC, Lima EC, Allaudeen N, Rajan S (2016) Application of graphene-based materials for adsorption of pharmaceutical traces from water and wastewater—a review. Desalin Water Treat 57:27573–27586
19. Kasperiski FM, Lima EC, Umpierres CS, dos Reis GS, Thue PS, Lima DR, Dias SLP, Saucier C, da Costa JB (2018) Production of porous activated carbons from *Caesalpinia ferrea* seed pod wastes: highly efficient removal of captopril from aqueous solutions. J Clean Prod 197:919–929
20. Leite AB, Saucier C, Lima EC, dos Reis GS, Umpierres CS, Mello BL, Shirmardi M, Dias SLP, Sampaio CH (2018) Activated carbons from avocado seed: optimization and application for removal several emerging organic compounds. Environ Sci Pollut Res 25:7647–7661
21. Umpierres CS, Thue PS, dos Reis GS, de Brum IAS, Lima EC, de Alencar WA, Dias SLP, Dotto GL (2018) Microwave activated carbons from Tucumã (*Astrocaryum aculeatum*) waste for efficient removal of 2-nitrophenol from aqueous solutions. Environ Technol 39:1173–1187
22. Torrellas SÁ, Lovera RG, Escalona N, Sepúlveda C, Sotelo JL, García J (2015) Chemical-activated carbons from peach stones for the adsorption of emerging contaminants in aqueous solutions. Chem Eng J 279:788–798
23. Cunha MR, Lima EC, Cimirro NFGM, Thue PS, Dias SLP, Gelesky MA, Dotto GL, dos Reis GS, Pavan FA (2018) Conversion of Eragrostis plana Nees leaves to activated carbon by microwave-assisted pyrolysis for the removal of organic emerging contaminants from aqueous solutions. Environ Sci Pollut Res 25:23315–23327
24. Lladó J, Lao-Luque C, Ruiz B, Fuente E, Solé-Sardans M, Dorado AD (2015) Role of activated carbon properties in atrazine and paracetamol adsorption equilibrium and kinetics. Process Saf Environ Prot 95:51–59
25. Puchana-Rosero MJ, Adebayo MA, Lima EC, Machado FM, Thue PS, Vaghetti JCP, Umpierres CS, Gutterres M (2016) Microwave-assisted activated carbon obtained from the sludge of tannery-treatment effluent plant for removal of leather dyes. Colloid Surf A 504:105–115
26. Baquião AC, Zorzete P, Reis TA, Assunção E, Vergueiro S, Correa B (2012) Mycoflora and mycotoxins in field samples of Brazil nuts. Food Control 28:224–229
27. Yang J (2009) Brazil nuts and associated health benefits: a review. Food Sci Technol 42:1573–1580
28. NORMAN (2019) The network of reference laboratories, research centres, and related organisations for monitoring of emerging environmental substances. www.norman-network.net
29. Wang X, Miao J, Pan L, Li Y, Lin Y, Wu J (2019) Toxicity effects of p-choroaniline on the growth, photosynthesis, respiration capacity, and antioxidant enzyme activities of a diatom, *Phaeodactylum tricornutu*. Ecotox Environ Saf 169:654–661
30. Koenig CM, Beevers C, Pant K, Young RR (2018) Assessment of the mutagenic potential of para-chloroaniline and aniline in the liver, spleen, and bone marrow of Big Blu® rats with micronuclei analysis in peripheral blood. Environ Mol Mutagen 59:785–797
31. Thue PS, Adebayo MA, Lima EC, Sieliechi JM, Machado FM, Dotto GL, Vaghetti JCP, Dias SLP (2016) Preparation, characterization, and application of microwave-assisted activated carbons from wood chips for removal of phenol from aqueous solution. J Mol Liq 223:1067–1080
32. Thue PS, Lima EC, Sieliechi JM, Saucier C, Dias SLP, Vaghetti JCP, Rodembusch FS, Pavan FA (2017) Effects of first–row transition metals and impregnation ratios on the physicochemical properties of microwave-assisted activated carbons from wood biomass. J Colloid Interface Sci 486:163–175
33. Thommes M, Kaneko K, Neimark AV, Olivier JP, Rodriguez-Reinoso F, Rouquerol J, Sing KSW (2015) Physisorption of gases, with special reference to the evaluation of surface area and pore size distribution (IUPAC Technical Report). Pure Appl Chem 87:1051–1069
34. Jagiello J, Thommes M (2004) Comparison of DFT characterization methods based on N_2, Ar, CO_2, and H_2 adsorption applied to carbons with various pore size distributions. Carbon 42:1227–1232
35. Fröhlich AC, Foletto EL, Dotto GL (2019) Preparation and characterization of $NiFe_2O_4$/activated carbon composite as a potential magnetic adsorbent for removal of ibuprofen and ketoprofen pharmaceuticals from aqueous solutions. J Clean Prod 229:828–837
36. Kim YS, Yang SJ, Lim HJ, Kim T, Lee K, Park CR (2012) Effects of carbon dioxide and acidic carbon compounds on the analysis of Boehm titration curves. Carbon 50:1510–1516
37. Wamba AGN, Ndi SK, Lima EC, Kayem JG, Thue PS, Costa TMH, Quevedo AB, Benvenutti EV, Machado FM (2019) Preparation, characterization of titanate nanosheet–pozzolan nanocomposite and its use as an adsorbent for removal of diclofenac from simulated hospital effluent. J Taiwan Inst Chem Eng 102:321–329
38. de Oliveira Carvalho C, Rodrigues DLC, Lima EC, Umpierres CS, Caicedo DF, Machado FM (2019) Kinetic, Equilibrium, and thermodynamic studies on the adsorption of ciprofloxacin by activated carbon produced from Jerivá (*Syagrus Romanzoffiana*). Environ Sci Pollut Res 26:4690–4702
39. Lima EC, Barbosa F Jr., Krug FJ, Guaita U (1999) Tungsten-rhodium permanent chemical modifier for lead determination in digests of biological materials and sediments by electrothermal atomic absorption spectrometry. J Anal At Spectrom 14:1601–1605
40. Lima EC, Brasil JL, Santos AHDP (2003) Evaluation of Rh, Ir, Ru, W-Rh, W-Ir, and W-Ru as permanent modifiers for the determination of lead in ashes, coals, sediments, sludges, soils, and freshwaters by electrothermal atomic absorption spectrometry. Anal Chim Acta 484:233–242
41. Lima EC, Barbosa F Jr., Krug FJ (2000) The use of tungsten–rhodium permanent chemical modifier for cadmium determination in decomposed samples of biological materials and sediments by electrothermal atomic absorption spectrometry. Anal Chim Acta 409:267–274
42. Lima EC, Krug FJ, Nóbrega JA, Nogueira ARA (1998) Determination of ytterbium in animal faeces by tungsten coil electrothermal atomic absorption spectrometry. Talanta 47:613–623
43. Lima EC, Fenga PG, Romero JR, de Giovani W (1998) Electrochemical behaviour of [Ru(4,4'-Me2bpy)2(PPh3)(H2O)](ClO4)2 in homogeneous solution and incorporated into carbon paste electrodes. Application to oxidation of benzylic compounds. Polyhedron 17:313–318
44. Lima EC, Adebayo MA, Machado FM (2015) Chapter 3: kinetic and equilibrium models of adsorption, in carbon nanomaterials as adsorbents for environmental and biological applications. In: Bergmann CP, Machado FM (eds). Springer International Publishing, New York, pp 33–69
45. Schwarz GGE (1978) Estimating the dimension of a model. Ann Stat 6:461–464
46. Lima EC, Hosseini-Bandegharaei A, Moreno-Piraján JC, Anastopoulos I (2019) A critical review of the estimation of the thermodynamic parameters on adsorption equilibria. Wrong use of

equilibrium constant in the Van't Hoof equation for calculation of thermodynamic parameters of adsorption. J Mol Liq 273:425–434
47. Mondal S, Majumder SK (2019) Synthesis of phosphate functionalized highly porous activated carbon and its utilization as an efficient copper (II) adsorbent. Korean J Chem Eng 36:701–712
48. Bhomick PC, Supong A, Karmaker R, Baruah M, Pongener C, Sinha D (2019) Activated carbon synthesized from biomass material using single-step KOH activation for adsorption of fluoride: experimental and theoretical investigation. Korean J Chem Eng 36:551–562
49. Lima DR, Hosseini-Bandegharaei A, Thue PS, Lima EC, de Albuquerque YRT, dos Reis GS, Umpierres CS, Dias SLP, Tran HN (2019) Efficient acetaminophen removal from water and hospital effluents treatment by activated carbons derived from Brazil nutshells. Colloids Surf A Physicochem Eng Asp 583:1–12
50. Thue PS, Sophia AC, Lima EC, Wamba AGN, de Alencar WS, dos Reis GS, Rodembusch FS, Dias SLP (2018) Synthesis and characterization of a novel organic-inorganic hybrid clay adsorbent for the removal of Acid Red 1 and Acid Green 25 from aqueous solutions. J Clean Prod 171:30–44
51. Chang R, Thoman JW Jr. (2014) Chapter 17-Intermolecular forces in "Physical Chemistry for Chemical Sciences". University Science Books, Mill Valley, pp 779–808
52. Lipkowski P, Koll A, Karpfen A, Wolschann P (2002) An approach to estimate the energy of the intramolecular hydrogen bond. Chem Phys Lett 10:256–263
53. Skoog DA, Holler FJ, Crouch SR (2007) Principles of instrumental analysis, Thompson, pp 376–378
54. Anbia M (2015) S, Khoshbooei, Functionalized magnetic MCM-48 nanoporous silica by cyanuric chloride for removal of chlorophenol and bromophenol from aqueous media. J Nanostruct Chem 5:139–146
55. Oh SY, Seo YD (2016) Sorption of halogenated phenols and pharmaceuticals to biochar: affecting factors and mechanisms. Environ Sci Pollut Res 23:951–961
56. Oh SY, Seo YD (2019) Factors affecting the sorption of halogenated phenols onto polymer/biomass-derived biochar: Effects of pH, hydrophobicity, and deprotonation. J Environ Manag 232:145–152
57. Koyuncu H, Kul AR (2019) Removal of aniline from aqueous solution by activated kaolinite: kinetic, equilibrium and thermodynamic studies. Colloids Surf A 569:59–66
58. Yang K, Wu WH, Jing QF, Jiang W, Xing BS (2010) Competitive adsorption of naphthalene with 2,4-dichlorophenol and 4-chloroaniline on multiwalled carbon nanotubes. Environ Sci Technol 44:3021–3027